Water Supply

Water Supply Vol 22 No 1, 779 doi: 10.2166/ws.2021.232

Enhanced fluoride removal from drinking water in wide pH range using La/Fe/Al oxides loaded rice straw biochar

Nan Zhou, Xiangxin Guo, Changqing Ye*, Ling Yan, Weishi Gu, Xiangrong Wu, Qingwen Zhou, Yuhuan Yang, Xiaoping Wang and Qiwei Cheng

School of Public Health, Nantong University, Nantong 226019, Jiangsu, People's Republic of China
*Corresponding author. E-mail: cqye@ntu.edu.cn

CY, 0000-0003-0523-3658

ABSTRACT

A novel and highly efficient adsorbent was prepared by loading La/Fe/Al oxides onto rice straw biochar (RSBC), which was tested for the ability to remove fluoride from drinking water. Characterized by SEM, XRD, Zeta potential and FTIR, it was found that the ternary metal oxides were successfully loaded on the surface of biochar in amorphous form, resulting in the formation of hydroxyl active adsorption sites and positive charges, which played a synergistic role in fluoride removal. Through batch adsorption tests, key factors including contact time, initial fluoride concentration, initial pH and co-existing anions effects were investigated. Results showed that the tri-metallic modified biochar (La/Fe/Al-RSBC) had excellent fluoride removal performance with an adsorption capacity of 111.11 mg/g. Solution pH had little impact on the removal of fluoride, the adsorbent retained excellent fluoride removal capacity in a wide pH range of 3.0–11.0. The co-existing anions had almost no effect on the fluoride removal by La/Fe/Al-RSBC. In addition, La/Fe/Al-RSBC could be regenerated and reused. Electrostatic adsorption and ion exchange were responsible for this adsorption behavior. These findings suggested the broad application prospect of a prepared biochar adsorbent based on rare earth and aluminum impregnation for the fluoride removal from drinking water.

Key words: adsorption, aluminum, biochar, fluoride removal, iron, lanthanum

HIGHLIGHTS

- A novel tri-metal oxide loaded rice straw biochar (La/Fe/Al-RSBC) was successfully prepared by simple co-precipitation.
- La/Fe/Al-RSBC has excellent fluoride adsorption performance with wide pH range.
- The mechanism of fluoride adsorption involves in electric attraction and ion exchange.

GRAPHICAL ABSTRACT

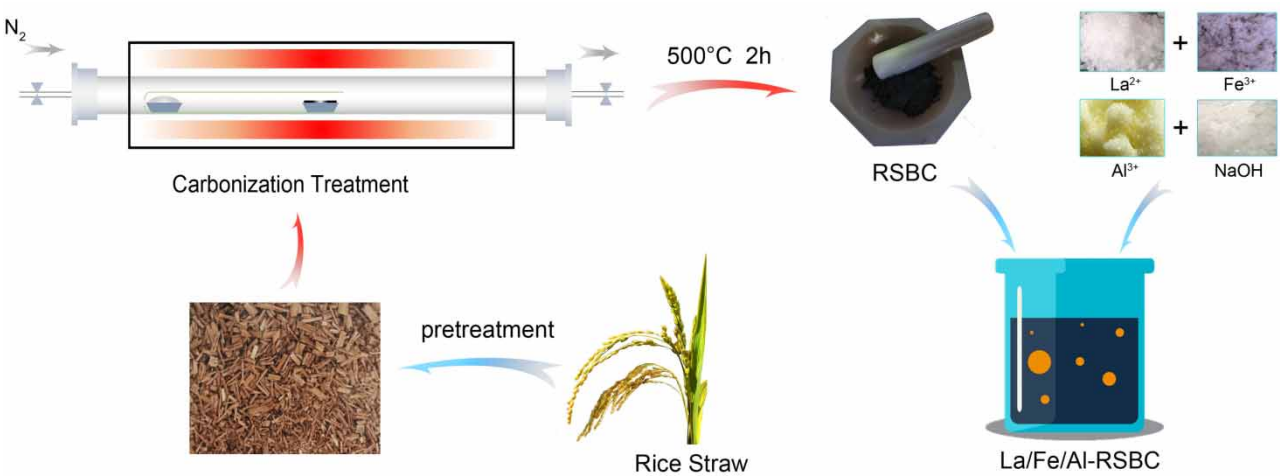

INTRODUCTION

Fluoride is one of the most abundant anions in drinking water, and its effect on the human body depends on the dose of fluoride ion (Zhang *et al.* 2014). Human body intake of low-dose fluoride ion can prevent dental caries (Mahramanlioglu *et al.* 2002). When the content of fluoride ion is too high in drinking water, it will lead to dental fluorosis, skeletal fluorosis, and nerve damage (Zhang & Huang 2019). In severe cases, it may endanger human health or even life (Ruan *et al.* 2017). The World Health Organization (WHO) stipulates that the acceptable fluoride concentration in drinking water is between 0.5 and 1.5 mg/L (Wang & Reardon 2001). According to reports, more than 200 million people worldwide are drinking water with a fluoride concentration exceeding 1.5 mg/L (Yadav *et al.* 2013a). Because of some environmental and human factors, China has become one of the countries suffering from fluorosis in the world. At present, about 50 million people in China are drinking high-fluoride water, mainly in the northwest and central regions (Wen *et al.* 2013). High fluoride in drinking water has become a recognized major public health hazard in many parts of the world (Loganathana *et al.* 2013). Therefore, it is essential to develop effective defluoridation technologies to protect people's drinking water safety and public health.

At present, there are many effective methods to remove high fluoride, such as adsorption (Rajkumar *et al.* 2015), precipitation (Zhang *et al.* 2012), ion exchange (Cui *et al.* 2011), membrane filtration (Yadav *et al.* 2013b) and electrodialysis (Lahnid *et al.* 2008). Compared to other methods such as precipitation (Meenakshi & Maheshwari 2006) and ion exchange (Piyush *et al.* 2012), the adsorption method is still considered as the mainstream technology for fluoride removal research and application due to its relatively low cost, environmental friendliness and easy operation (Medellin-Castillo *et al.* 2014).

In recent years, the fluoride removal of activated alumina in drinking water has been extensively studied, and alumina has become a recognized fluoride adsorbent (Pant 2004; Pietrelli 2005). Alumina is a porous substance with great fluoride adsorption performance, low cost, and broad application (Farrah *et al.* 1987). Aluminum (hydroxide) oxide has the characteristic of fluoriphilic and positive charge on its surface, and it is easy to form a pore structure through process control. Therefore, the aluminum-based materials can be selected as the main body. However, aluminum products are active in a narrow pH range (Bhatnagar *et al.* 2011), and activated alumina has a high cost and the risk of aluminum dissolution. Therefore, it is urgent to modify the traditional adsorbents and develop novel and efficient fluoride adsorbents.

Methods to improve the fluoride removal by aluminum-based adsorbents can be roughly divided into two categories. One is aluminum-excluded metal doping; for example, aluminum-based layered double metal hydroxide (LDH) was prepared in a way where aluminum oxides are doped with Fe, Zr, Ca and Mg (Maliyekkal *et al.* 2008; Chai *et al.* 2013; Wang *et al.* 2016). The other is loading of carbon-based materials, in which aluminum or other metals can be loaded on carbon-based materials. Biochar loading has been widely reported recently (Habibi *et al.* 2018; Zhang *et al.* 2019; Yan *et al.* 2021). Biochar is a product obtained by the pyrolysis of biomass such as crop straw, rice husk, tea residue, bone, vegetables and other agricultural wastes under high temperature (generally <700 °C) in an anoxic or anaerobic environment (Ahmed *et al.* 2016). Biochar has the potential to be used in the preparation of adsorbents for fluoride removal because of its large specific surface area, complex pore structure and abundant functional groups (Mian & Liu 2018). Rice straw resources are abundant in South China, which is conducive to carbonization (Ganvir & Das 2011; Fu *et al.* 2018). Therefore, this study will also use rice straw as the main biomass to synthesize rice straw biochar. However, the ability of biochar to remove fluoride is limited, and needs to be enhanced through modification (Cai *et al.* 2015; Chen *et al.* 2016), especially through aluminum modification. The main function of biochar is to load and disperse aluminum. The point of zero charge (pH_{pzc}) of aluminum hydroxide is high, and a large number of aluminum hydroxide are dispersed on the surface of the biochar. Therefore, the biochar loaded with aluminum has high AEC at high pH, which can effectively remove fluoride in the alkaline range (Lawrinenko *et al.* 2017).

In recent years, some rare earth elements have attracted growing attention because of their excellent fluoride adsorption capacity, little pollution and easy operation (Wang *et al.* 2015; Peng *et al.* 2017; Jiang *et al.* 2019). Wang *et al.* (2018a, 2018b) prepared a novel Fe-La composite adsorbent for fluoride and phosphate removal simultaneously. Therefore, the fluoride removal performance of the original iron-based adsorbent is significantly improved through doping rare earth elements. The rule is also applicable for aluminum-based adsorbents. Wang *et al.* (2017a) prepared an Mg-Al-La tri-metal oxide compound, the maximum adsorption capacity of fluoride being 31.72 mg/g when the pH value is between 4.0–10.0; Jiang *et al.* (2019) successfully prepared a laminated nanocomposite of Y-Zr-Al with a significantly high surface area of 256.6 m^2/g, the maximum adsorption capacity of fluoride being 31.0 mg/g when the pH value is 7.0; Jian *et al.* (2018) prepared Al-Zr-La tri-metal hydroxide, which removed fluoride at pH 3.0 with a maximum fluoride adsorption capacity of 90.48 mg/g. These studies show that aluminum-based adsorbents have better fluoride removal capacity after doping rare

earth elements, and rare earth-doped biochar has also attracted much attention. For example, lanthanum-loaded pomelo peel biochar (PPBC-La) can effectively remove fluoride (Wang *et al.* 2018a, 2018b). As mentioned above, aluminum modified biochar has good fluoride removal potential, and rare earth element doping on this basis is expected to further enhance the fluoride removal performance of the new adsorbent. However, up to now, there has been no report on this aspect.

In order to obtain a novel efficient and broad-spectrum fluoride removal adsorbent, rare earth of lanthanum doping on aluminum and iron modified biochar, which was derived from rice straw biomass, is investigated in this study, and the optimization of preparation, physico-chemical properties and fluoride removal performance are studied. Furthermore, the adsorption mechanism of the adsorbent for fluoride removal is discussed.

METHODS AND EXPERIMENTAL

Materials and reagents

All reagents including $LaN_3O_9{\cdot}6H_2O$, Fe $(NO_3)_3{\cdot}9H_2O$, $AlCl_3{\cdot}6H_2O$, NaF, NaOH, KCl, KNO_3, K_2SO_4, $NaHCO_3$, were commercially available from Sinopharm Chemical Reagent Co., Ltd (China) of analytical grade and were used without further purification.

The rice straw was collected from a local farm in Nantong City in south China. The collected rice straw was washed, crushed and calcined at 500 °C for 2 h under the protection of N_2, and then cooled to room temperature naturally. Finally, the biochar derived from rice straw (RSBC) was ground into powder of 100 mesh and placed in a sealed bag.

Preparation of adsorbent

La-Fe-Al composite with different La (III), Fe (III) and Al (III) contents were synthesized by the co-precipitation method. According to the preset molar ratio of La, Fe and Al, the corresponding metal salt was weighed and dissolved in a beaker with 50 mL deionized water. The molar ratios of different metals were set as follows, La: Fe: Al = 1:1:1; 1:1:3; 1:2:3; 1:3:1; 2:1:1; 2:1:3, respectively, La: Fe = 1:1; La: Al = 1:3; Fe: Al = 1:3. 1 g of RSBC was added into the above 50 mL metal salt solutions with different molar ratios, and the pH values were adjusted using 5 M NaOH solution, then stirred for 12 h. The suspension was centrifuged at 12,000 rpm for 5 minutes, washed twice with distilled water and absolute alcohol respectively, and dried at 110 °C for 4 h. Finally, after cooling naturally to room temperature, the modified biochar was ground, sieved under 100 mesh and placed in a sealed bag. The ternary metals-modified biochar was labeled as La/Fe/Al-RSBC, and bimetallic biochar as La/Fe-RSBC, La/Al-RSBC and Fe/Al-RSBC.

Characterization of samples

The surface morphology and other physical characteristics of the adsorbent were observed by field emission scanning electron microscopy (FESEM, Gemini SEM 300). The elemental composition of the adsorbent was analyzed by energy dispersive spectroscopy (EDS). The crystal phases of the samples were determined by X-ray diffraction (XRD, Ultima IV). The scanning rate was 2°/min and the diffraction angle was 5° to 85°. The surface charge of the sample was measured by ZS90 particle size analysis and Zeta potential analyzer (Zetasizer Nano ZS90). Fourier transform infrared spectroscopy (FTIR, Nicolet IS 50 + IN 10) was used to analyze the changes of the functional groups on the surface of the adsorbent before and after adsorption. The XPS spectra were referenced by setting 284.8 eV for the C (1 s) to eliminate with an Al anode (X-ray voltage 12 kV, 72 W, X-ray energy 1,486.6 eV).

Adsorption experiments

The fluoride stock solution was prepared with distilled water using NaF. Generally, the adsorption experiment was carried out in 50 mL centrifuge tubes, which contained 40 mg of adsorbent and 40 mL of fluoride solution, and then the tube was shaken in a constant temperature vibrator at 25 °C at a speed of 150 rpm for 24 h. Unless otherwise specified, the adsorbent dose for all experiments was 1 g/L. The pH value was adjusted to 7.0 ± 0.2 using dilute HCl or NaOH solution. After the adsorption experiment, the adsorbent was separated from the solution by filtration through a 0.45 μm membrane, and the residual fluoride concentration in solution was measured by the fluoride ion selective electrode (PXSJ-216F).

The studies of the adsorption isotherm of La/Fe/Al-RSBC were carried out by changing the initial fluoride concentration of adsorption system in the range of 6–160 mg/L. The Langmuir and Freundlich isotherm models were used to fit the experimental data. Adsorption kinetics experiments were performed at different contact times (10–600 min), the initial fluoride concentration was 6 mg/L, and the total suspension volume was 2 L. At predetermined time intervals, 20 mL of the

supernatant was drawn by syringe while stirring and filtered to determine the remaining fluoride concentrations. Pseudo-first-order and pseudo-second-order kinetics models were used to fit the data. The formulas for kinetic and isotherm models are presented in supplementary materials.

Further, in the study of the effects of pH experiments, the initial pH value varied from 3.0 to 11.0, initial concentration was 6 mg/L. The individual effect of different ions, such as Cl^-, SO_4^{2-}, NO_3^- and HCO_3^-, on fluoride adsorption by La/Fe/Al-RSBC was also studied. The experiment was carried out under a binary system, which contained 6 mg/L F^- paired with 1, 6 and 60 mg/L of each competing ion, respectively. The initial adsorbent dose was 1.0 mg/L. The initial solution pH was 7.0 $\pm$ 0.2.

Regeneration study

In the regeneration process, the used La/Fe/Al-RSBC was soaked in 40 mL 0.1M NaOH solution and agitated overnight at room temperature. Subsequently, the adsorbent was separated, washed, and dried. To investigate the reusability of La/Fe/Al-RSBC, typical adsorption experiment was performed three cycles after regeneration.

RESULTS AND DISCUSSION

Optimize modification conditions

The fluoride adsorption capacities of adsorbents prepared with different La: Fe: Al molar ratios were compared. The results are shown in Figure 1(a). It can be seen that the different metal molar ratios could relatively affect the adsorption capacity. According to the adsorption capacity of adsorbents, the order of La: Fe: Al molar ratio is as follows, 1:3:1 < 1:1:1 < 1:2:3 ~ 2:1:1 < 2:1:3 < 1:1:3. The adsorbent with the La: Fe: Al ratio of 1:1:3 was the most effective fluoride adsorbent. It showed that lanthanum and aluminum can promote fluoride removal more than iron, which could be further confirmed in bi-metal modified biochar systems. From Figure 1(b), among the three types of bi-metal modified biochar, fluoride removal of biochar modified by La/Al was much higher than by Fe/Al, and La/Fe was between the other two types. It was evident that the adsorbents containing La had high fluoride adsorption capacity, and the adsorbents containing Fe had less fluoride adsorption capacity. Further, as evident from Figure 1(b), the ternary metal adsorbent with corresponding ratios was more effective than binary metal adsorbents, indicating tri-metal modification could promote the fluoride removal significantly than bi-metal modification with strengthened synergistic effects. Similarly synergistic effects could be found by the study of Layered Y-Zr-Al tri-metallic nanocomposites (Jiang *et al.* 2019). Therefore, the optimized metals types and metal molar ratio for the modified biochar preparation was chosen as La: Fe: Al = 1:1:3. And this type of modified biochar, or La/Fe/Al-RSBC for short, was further studied.

Figure 1(c) showed the effect of pH value during the preparation of La/Fe/Al-RSBC with La: Fe: Al molar ratio of 1:1:3. It could be seen that when the pH value was lower than 8.0, the adsorption capacity of fluoride increased with the increase of pH value, but the fluoride removal decreased sharply while the pH increased to 10.0. It was evident that the pH value in the preparation process remarkably affected the fluoride adsorption capacity of the modified biochar. The main reason was that when the pH value was too high, the precipitation speed was too fast, which led to the formation of impurities or the precipitation of some metal ions. When the pH value was too low, as the content of by-products increased, the components with adsorption activity decreased, resulting in the decrease of adsorption performance of products. Therefore, the results showed the optimum pH value during the preparation should be 8.0.

Characterization

The surface morphology of the RSBC, La/Fe/Al-RSBC, and the sample after adsorption, denoted as La/Fe/Al-RSBC-F, were analyzed by SEM (Figure 2). The RSBC had a relatively smooth surface (Figure 2(a)), while the La/Fe/Al-RSBC surface was rough and produced some small amorphous particles (Figure 2(b)). Loose and porous flocculent materials were observed at high magnification (Figure 2(c)). After impregnation by metals, the surface area of the La/Fe/Al-RSBC increased. This indicated that granular material may form on the surface of the La/Fe/Al-RSBC and that the surface area increased after modifying with La/Fe/Al metals. The SEM-EDS spectrum showed that C and O were the main elements on the surface of the RSBC (Fig. S1a). In contrast, the new presence of La, Fe, and Al peaks was found in the La/Fe/Al-RSBC, these metals might exist on the surface in the form of metal oxides or hydroxides (Fig. S1b). Morphology and structural characterization strongly support that the trimetallic biochar has been successfully synthesized.

After adsorption of fluoride, SEM showed that the surface of the adsorbent changed and a laminated material was observed (Figure 2(d)). Presence of fluoride in La/Fe/Al-RSBC after adsorption was also observed in the SEM-EDS spectrum (Fig. S1c). This finding suggested that the La/Fe/Al-RSBC adsorbed fluoride successfully from drinking water.

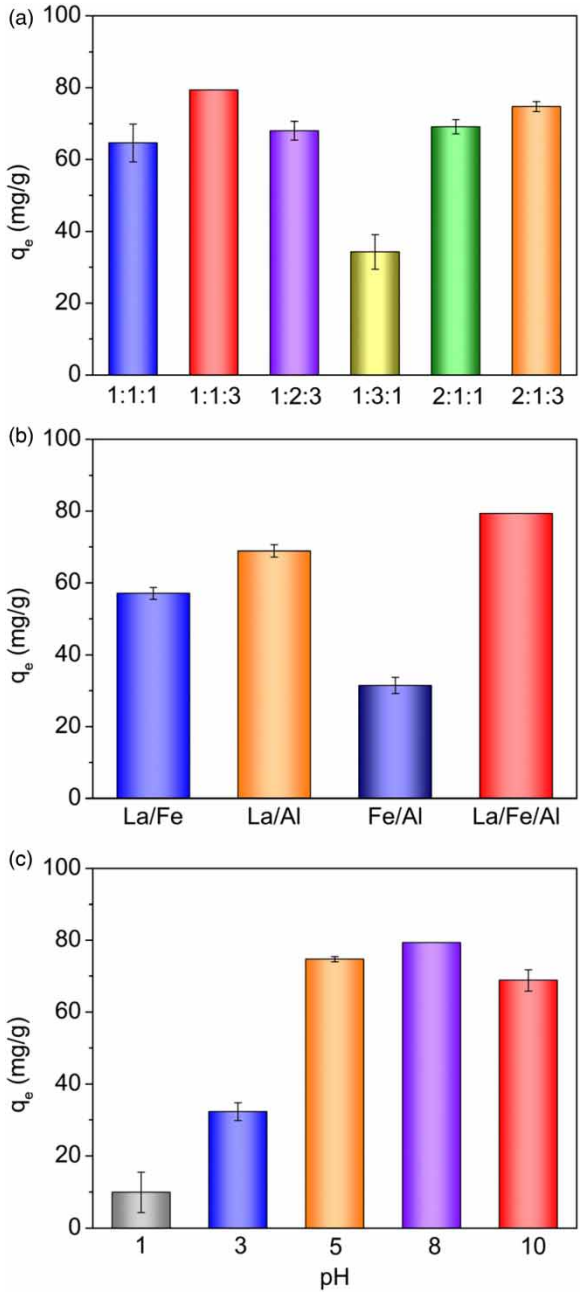

Figure 1 | (a) Adsorption of fluoride on the as-prepared adsorbent at different La/Fe/Al molar ratios. (b) Fluoride adsorption capacity comparison of binary and ternary metal adsorbents (adsorbent dose 1 g/L, contact time 24 h, initial concentration 80 mg/L, pH 7.0 $\pm$ 0.2). (c) Effect of preparation pH on fluoride adsorption (pH = 1.0 is the pH value of the mixed solution without sodium hydroxide in the preparation process).

The BET-specific surface area and pore size distribution of RSBC and La/Fe/Al-RSBC were calculated using N_2 adsorption/desorption isotherms (Figure 3). The BET surface area of RSBC was 2.59 m^2/g; conversely, the La/Fe/Al-RSBC was 95.36 m^2/g (Table 1). Based on the Barrett–Joyner–Halenda (BJH) method, the average pore diameters of RSBC and La/Fe/Al-RSBC were 12.01 and 12.49 nm, respectively. Additionally, the inclusion of metal salts can facilitate the BET surface area of biochar.

The XRD patterns of the RSBC, bi-metallic and tri-metallic RSBC were recorded to study the crystalline structure (Fig. S2). The XRD pattern of the RSBC showed several sharp peaks that correspond to mineral phases (Liu *et al.* 2016), mainly SiO_2

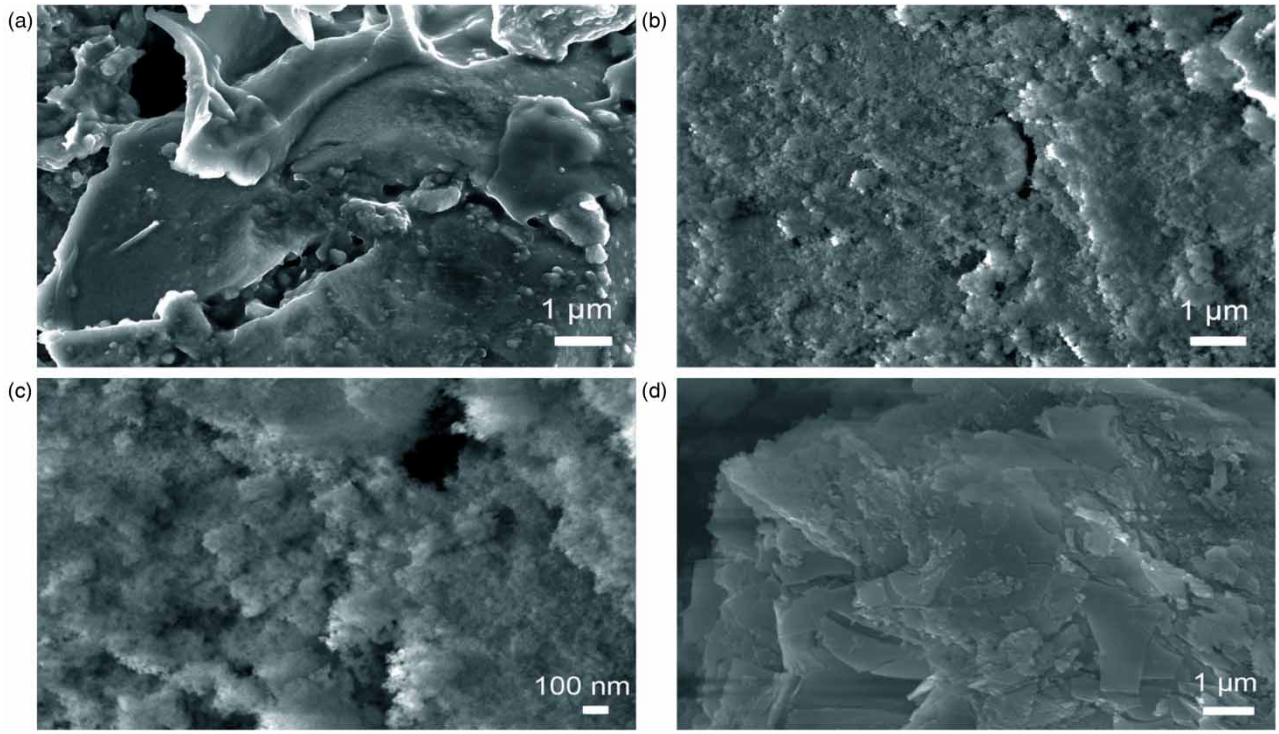

Figure 2 | SEM images of (a) RSBC, (b, c) La/Fe/Al-RSBC and (d) La/Fe/Al-RSBC-F.

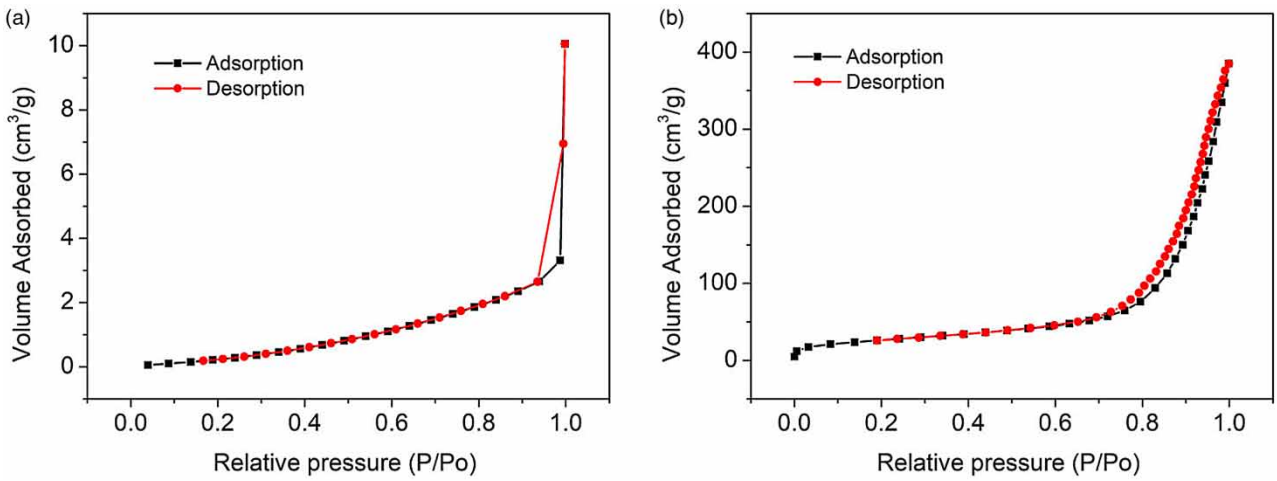

Figure 3 | N_2 adsorption/desorption isotherms of (a) RSBC and (b) La/Fe/Al-RSBC.

Table 1 | Summary of BET analysis results of RSBC and La/Fe/Al-RSBC

	RSBC	La/Fe/Al-RSBC
BET surface area (m^2/g)	2.59	95.36
Pore volume (cm^3/g)	0.012	0.611
Pore diameter (nm)	12.01	12.49

and KCl. Interestingly, these peaks disappeared after modification with metal salts. This could be due to the fact that minerals can be easily dissolved by adding NaOH during the modification process. In the XRD patterns of La/Fe/Al-RSBC, La/Fe-RSBC, and Fe/Al-RSBC, there was a characteristic peak of $Fe_3O(OH)$ at $2\theta = 26°$, but there were no distinct peaks for lanthanum and aluminum oxide, suggesting that the lanthanum and aluminum oxides on the surface of the loaded biochar were amorphous. Figure 1(b) also showed that the amorphous material in La/Fe/Al-RSBC and La/Al-RSBC had better adsorption performance than crystalline materials La/Fe-RSBC and Fe/Al-RSBC. This indicated amorphous materials had more active sites and larger specific surface area than crystalline materials, which rendered them good adsorption performance (Jain & Jayaram 2009). Therefore, the loaded La/Fe/Al-RSBC was expected to be an effective adsorbent to remove fluoride.

The FTIR spectra of the RSBC, bi-metallic and tri-metallic RSBC are shown in Figure 4. The broad peaks around 3,396 cm^{-1} were found for all the modified samples in addition to the raw RSBC, which was due to the hydroxyl stretching of the adsorbent.

This demonstrated that plenty of hydroxyl could be produced on the surface of biochar through metallic modification, which contributed to the active sites of the adsorbents. The adsorption band around 1,417 cm^{-1} was ascribed to the asymmetric stretching bending vibration of $-CH_3$. In all samples, the peak around 1,065 cm^{-1} corresponded to stretching vibration of the Si-O-Si band resulting from the rice straw biomass.

Adsorption kinetics

The kinetics of fluoride adsorption of RSBC and La/Fe/Al-RSBC at pH 7 are shown in Figure 5(a). The RSBC reached the adsorption equilibrium within 30 minutes, and the equilibrium adsorption capacity was 0.38 mg/g. The La/Fe/Al-RSBC adsorption of fluoride increased rapidly in the initial stage. More than 95% fluoride could be adsorbed in the first 1 h, and equilibrium was reached in 2 h; the equilibrium adsorption capacity was 5.89 mg/g. The fast adsorption rate in the initial stage was likely due to the availability of a large number of active sites on the adsorbent surface (Mei *et al.* 2020). The adsorption process then gradually slowed down due to the reduction of the available adsorption sites and the accumulation of fluoride on the surface of the adsorbent (Awual *et al.* 2015).

Pseudo-first-order kinetic and pseudo-second-order models were used to analyze the kinetic data (Ho & Mckay 2000; Ho 2006) as shown in Fig. S3. Table 2 summarized the kinetic parameters calculated from the pseudo-first-order kinetic and pseudo-second-order models. It could be seen that the correlation coefficient values (R^2) obtained from the pseudo-second-order kinetic model for the RSBC and the La/Fe/Al- RSBC were 0.9959 and 1, respectively, much higher than pseudo-first-order model. The calculated equilibrium adsorption capacity was 5.90 when the initial fluoride concentration was 6 mg/L, which was in agreement with experimental equilibrium adsorption capacities. These findings indicated that the pseudo-second-order model was more suitable to predict the adsorption process of the adsorbent, which subsequently meant that the adsorption rate was controlled by chemical adsorption (Bakhtiari & Azizian 2015), it could be inferred that the adsorption of F^- on La/Fe/Al- RSBC was mainly chemical adsorption.

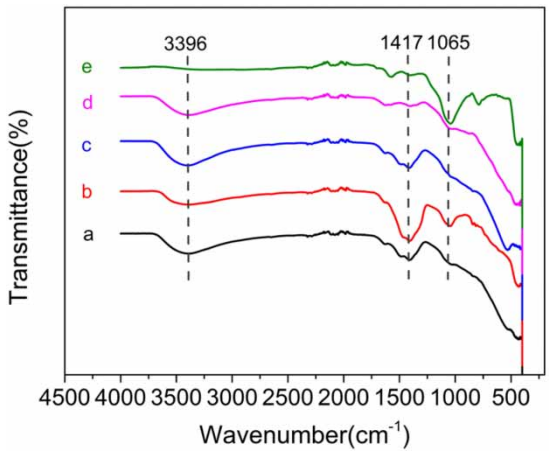

Figure 4 | FTIR spectra of (a) La/Fe/Al-RSBC, (b) La/Fe-RSBC, (c) La/Al-RSBC, (d) Fe/Al-RSBC and (e) RSBC.

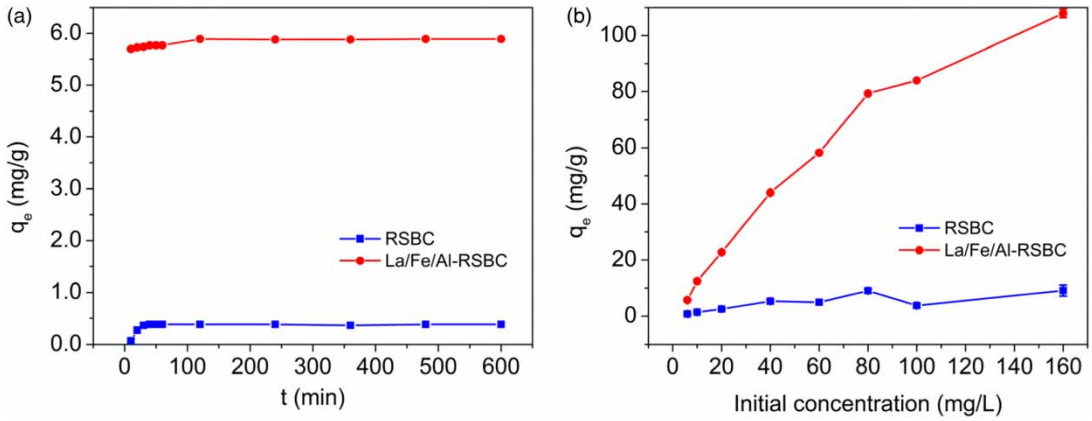

Figure 5 | (a) Effect of contact time (10–600 min) on the fluoride adsorption. (b) Effect of the initial fluoride concentration (6–160 mg/L) on fluoride adsorption. All reactions contained 1 g/L adsorbent and were at a pH of 7.0 ± 0.2.

Table 2 | Pseudo-first-order and pseudo-second-order kinetic models constants for adsorption of fluoride on adsorbents

		Pseudo-first-order kinetic model			Pseudo-second-order kinetic model		
Adsorbents	**Experimental capacity(mg/g)**	**k_1(1/min)**	**q_e(mg/g)**	**R^2**	**k_2(1/min)**	**q_e(mg/g)**	**R^2**
RSBC	0.38	0.058	1.13	0.9782	0.2805	0.39	0.9958
La/Fe/Al-RSBC	5.89	0.0043	5.16	0.8938	0.2296	5.90	1.0000

Adsorption isotherms

To further understand the adsorption performance, the adsorption isotherm of fluoride adsorption on the RSBC and La/Fe/Al-RSBC was compared. The adsorption isotherms at pH 7 were shown in Figure 5(b). The fluoride adsorption capacity of the RSBC tended to be stable, and the maximum adsorption capacity was 9.14 mg/g. The adsorption capacity of La/Fe/Al-RSBC increased with increasing initial fluoride concentration and stabled at high F^- concentration. When the initial fluoride concentration was low, the adsorption capacity increased rapidly due to sufficient active adsorption sites, and when the initial fluoride concentration increased to a higher concentration, the adsorption sites were limited and gradually reach saturation, therefore the adsorption capacity was increasing slowed down (Bansiwal *et al.* 2009; Wang *et al.* 2017b). The fluoride adsorption capacity of La/Fe/Al-RSBC increased from 5.75 mg/g to 107.87 mg/g as the initial concentration of fluoride increased from 6 mg/L to 160 mg/L, much higher than that of RSBC. Moreover, the residual F^- concentration could be reduced from the initial fluoride concentration of 6 mg/L to less than 1.5 mg/L, which was lower than the fluoride standard allowed by the World Health Organization.

Two basic isotherm models named Langmuir and Freundlich models were used to fit the present data (Fig. S3). Table 3 summarized the isotherm parameters calculated from the Langmuir and Freundlich models. It can be seen that for isotherm of the La/Fe/Al-RSBC, the correlation coefficient values of the Langmuir and Freundlich models were 0.994 and 0.768, respectively, indicating that the fluoride adsorption isotherm of the La/Fe/Al-RSBC followed the Langmuir model. The results were consistent with the previously reported model of fluoride removal by modified biochar adsorbent. On the contrary, the fluoride adsorption isotherm of the RSBC followed the Freundlich model with the correlation coefficient values of

Table 3 | Langmuir and Freundlich isotherm constants for adsorption of fluoride on adsorbents

		Langmuir isotherm			Freundlich isotherm		
Adsorbents	**Experimental capacity(mg/g)**	**q_0(mg/g)**	**b(L/mg)**	**R^2**	**n**	**k(mg/g)**	**R^2**
RSBC	9.14	10.85	0.014	0.515	1.43	3.634	0.860
La/Fe/Al-RSBC	107.87	111.11	0.319	0.994	2.21	24.210	0.768

0.860. The Langmuir model is based on the single-layer adsorption of the active site of the adsorbent (Abri *et al.* 2019), while the Freundlich model is based on adsorption on a heterogeneous surface (Tangsir *et al.* 2016). The results suggested that fluoride adsorbed on La/Fe/Al-RSBC followed single layer adsorption, and the active sites of the tri-metal modified biochar adsorbent played an important role. In contrast, the adsorption of fluoride onto the raw biochar was a heterogeneous adsorption, implying that pore structure of the RSBC might be the major adsorption site when not modified. The maximum adsorption capacity was calculated to be 111.11 mg/g.

By comparing with other previously reported fluoride adsorbents (Table 4), it can be found that the prepared tri-metallic modified La/Fe/Al-RSBC was superior to the majority of the biomass-based or tri-metallic adsorbents. Only MCH-La loaded with La showed a stronger absorption ability; however, the MCH-La was active in only a narrow pH range (in neutral solution), which would likely restrict further application. In contrast, the tri-metallic modified La/Fe/Al-RSBC overcame this shortcoming and consequently facilitated the practical application of the treatment of drinking water with excessive fluoride. The results might be due to the synergistic interaction between ternary metals and biochar in the adsorption.

Effect of pH on adsorption

It is well known that the pH value of aqueous solution can largely affect the adsorption performance. Figure 6(a) presents the effect of pH value on adsorption of fluoride on the RSBC and La/Fe/Al-RSBC. It can be seen that, in the range of 3.0 to 11.0, the pH value had almost little influence on the fluoride removal on La/Fe/Al-RSBC. However, when the pH value increased from 3.0 to 7.0, the fluoride removal on RSBC dramatically decreased. The quick reduction of the amount of fluoride adsorbed in pH >3.0 could be attributed to competition of hydroxyl ions with fluoride for adsorption sites.

From Figure 6(b) we can see at all measured pH values, the Zeta potential of the adsorbent of La/Fe/Al-RSBC was positive with positively charged functional groups on the surface, which was conducive to the adsorption of fluoride ions (Bhatnagar *et al.* 2011). The zeta potential of La/Fe/Al-RSBC remained above 30 mV at pH 3.0–8.4 but fell sharply to 0.0165 mV as the pH increased to 11.0. This finding indicated that the protons in the acidic suspension had little effect on the Zeta potential value of La/Fe/Al-RSBC, while the added -OH groups in the alkaline suspension could shield the positively charged functional groups on the adsorbent (Dong & Wang 2016). The F^- adsorption capacity of La/Fe/Al-RSBC showed a stable value at pH 2.8–5.2, which was in accordance with its corresponding Zeta potential, indicating electrostatic attraction force was one of the main controlling forces, especially in low pH conditions. However, when pH was higher than 8.0, the Zeta potential dramatically decreased, and the fluoride adsorption process of the La/Fe/Al-RSBC did not match the variation of Zeta potential values. This result demonstrated that electrostatic attraction was not the only reason for the adsorption of F^- on La/Fe/Al-RSBC, it might due to the abundant -OH functional groups on the adsorbent, which made it adsorb F^- through ion exchange (Ling *et al.* 2012). In short, pH had little effect on the adsorption of F^- by La/Fe/Al-RSBC adsorbent, indicating that the adsorbent had a widely applicable pH range.

Table 4 | Comparison of maximum adsorption capacity (Q_m) of different adsorbents toward fluoride ion

Adsorbent	pH	Q_m(mg/g)	References
Y-Zr-Al composite	7.0	31.0	Jiang *et al.* (2019)
Tea-Al-Fe	4.0–8.0	18.52	Cai *et al.* (2015)
Mg-Al-La tri-metal oxide	4.0–10.0	31.72	Wang *et al.* (2017a)
Al-Zr-La tri-metal hydroxide	3.0	90.48	Jian *et al.* (2018)
Zirconium-impregnated Camellia seed biochar	3.0–10.0	11.04	Mei *et al.* (2020)
PPBC-La	6.5	19.86	(Wang *et al.* 2017b)
MCH-La	7.0	136.78	Dong & Wang (2016)
Fe-La composite	3.8–7.1	27.42	Wang *et al.* (2018a, 2018b)
Bone biochar	8.0	5.05	Zhou *et al.* (2019)
Magnetic bone biochar	8.0	5.23	Zhou *et al.* (2019)
La/Fe/Al-RSBC	3.0–11.0	111.11	This study
RSBC	3.0	10.85	This study

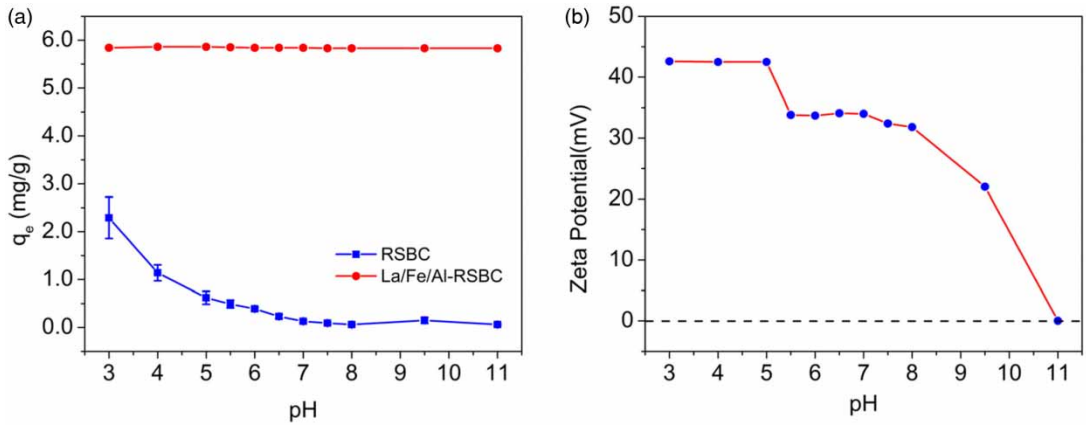

Figure 6 | Effect of pH on (a) fluoride removal capacity; (b) zeta potential of La/Fe/Al-RSBC. (adsorbent dose 1 g/L, contact time 24 h, initial concentration 6 mg/L).

Effect of co-existing anions

In actual water treatment, many anions commonly co-exist with fluoride ions; thus, it was important to investigate the interference of co-existing ions on fluoride adsorption. The effects of commonly present anions such as Cl^-, SO_4^{2-}, NO_3^- and HCO_3^- on fluoride adsorption capacity of La/Fe/Al-RSBC were investigated. As shown in Figure 7(a), the co-existing ions had little effect on the adsorption of F^- by the adsorbent. After the co-existing ion had been added, the fluoride removal rate of the adsorbent could still reach 94%, which showed that La/Fe/Al-RSBC had a strong anti-interference. This character has very important meaning in practical application.

Regeneration research

In order to study the fluoride adsorption performance of La/Fe/Al-RSBC after regeneration, three regeneration cycle adsorption experiments were tested and compared with the first adsorption experiment result of the adsorbent to verify the level of La/Fe/Al-RSBC regeneration performance, the results are shown in Figure 7(b). In the first adsorption, a fluoride removal rate of 97.75% was obtained. After the three regeneration cycles, the percentage of fluoride removal continuously decreased to 61.90%. This could be ascribed to the chemisorption of previously adsorbed fluoride on the La/Fe/Al-RSBC and some loss of adsorbents during the regeneration cycles (Zhang *et al.* 2019). Therefore, the results showed that La/Fe/Al-RSBC was more stable. It could be recycled many times, reducing the treatment cost, which provides the basis for the practical application of adsorbents.

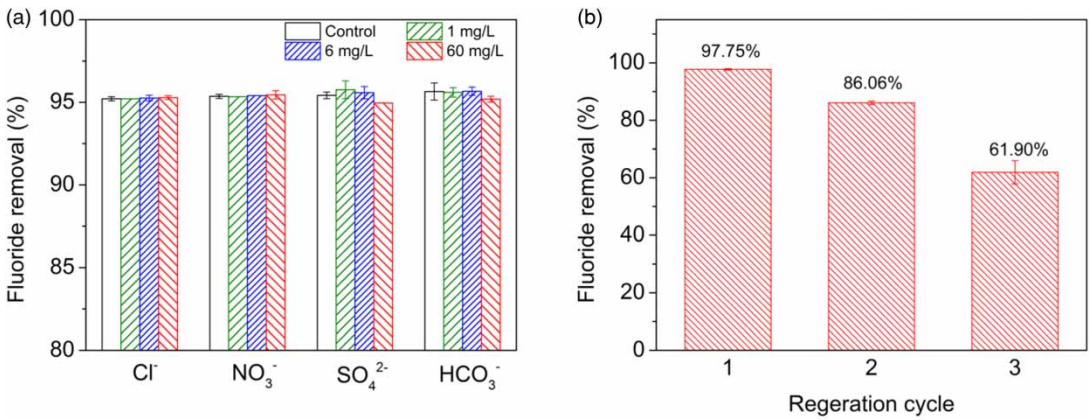

Figure 7 | (a) Effect of co-existing ions on fluoride adsorption by the La/Fe/Al-RSBC. (b) Reusing ability of the La/Fe/Al-RSBC adsorbent.

Adsorption mechanism

FTIR study

In order to explore the mechanism of adsorption of La/Fe/Al-RSBC, surface changes of functional groups were analyzed by FTIR. Figure 8 showed the FTIR spectra of La/Fe/Al-RSBC before and after adsorption. Before adsorption, the peak at 3,396 cm^{-1} was due to the stretching vibration of -OH on the adsorbent surface. However, the hydroxyl peak shifted to 3,373 cm^{-1} after adsorption, and the intensity weakened after adsorption, indicating that the hydroxyl groups participated in the adsorption reaction (Delgadillo-Velasco *et al.* 2017; Mei *et al.* 2020). The results showed that the ion exchange between the hydroxyl group and the fluoride ion could remove the fluoride.

Mean free energy of sorption

The equilibrium adsorption isotherm data of La/Fe/Al-RSBC at 298 K (pH = 7.0) were fitted to the Dubinin–Radushkevich isotherm model to calculate the mean free energy of sorption. The Dubinin–Radushkevich isotherm model was used to determine the main adsorption mechanism in the system (Mei *et al.* 2020).

The Dubinin–Radushkevich isotherm model of La/Fe/Al-RSBC at 298 K is shown in Figure S4, which indicates a good linear fitting with $R^2 = 0.9810$. It can be obtained from the figure that q_m was 82.47 mg/g and E was 10.91 kJ/mol. When the E value was less than 8 kJ/mol, the adsorption was considered as a physical adsorption process, and when the E value was in the range of 8–16 kJ/mol, the adsorption process was mainly controlled by ion exchange (Ho & Mckay 1998; Ajisha & Rajagopal 2014). The study found that the E value was in the range of 8–16 kJ/mol. Therefore, the results showed that the adsorption of fluoride on La/Fe/Al-RSBC was mainly an ion exchange process.

XPS study

XPS was used to investigate the sorbents before and after F^- adsorption, and the results are shown in Figure 9. As one can see in Figure 9(a), wide scan spectra indicated elements of La, Fe and Al exist in both adsorbents before and after fluoride adsorption. Furthermore, a new peak of F 1 s obviously appeared in F-loaded adsorbent, and the F content in Table 5 also increased from 0 to 1.82%, confirming the fluoride adsorption on the La/Fe/Al-RSBC. The content of O decreased from 57.24% to 54.84% after adsorption, which indicated that the -OH group participated in the process of fluorine adsorption. High resolution XPS spectrum of F (Figure 9(b)) indicated that the F 1 s peak in the La/Fe/Al-RSBC after adsorption was at 684.7 eV, and was higher than the 684.5 eV peak of NaF. Furthermore, high resolution XPS spectra of La, Fe and Al (Figure 9(c)–9(e)) indicated the peaks of La 3d, Fe 2p and Al 2p also shifted after fluoride adsorption. This suggested that La, Fe and Al participated in fluoride adsorption. Therefore, bimetallic Fe-O-Al and Fe-O-La bonds might be formed during the loading process. From above analysis, it could be inferred that Fe–Al oxide and Fe-La oxide might be not a simple mixture of Fe

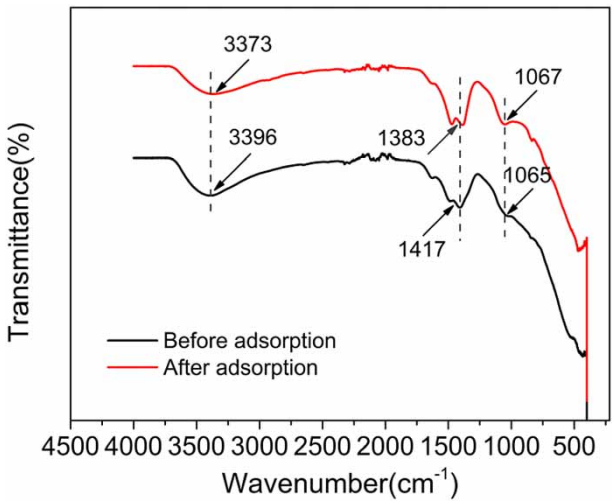

Figure 8 | FTIR spectra of La/Fe/Al-RSBC before and after fluoride adsorption.

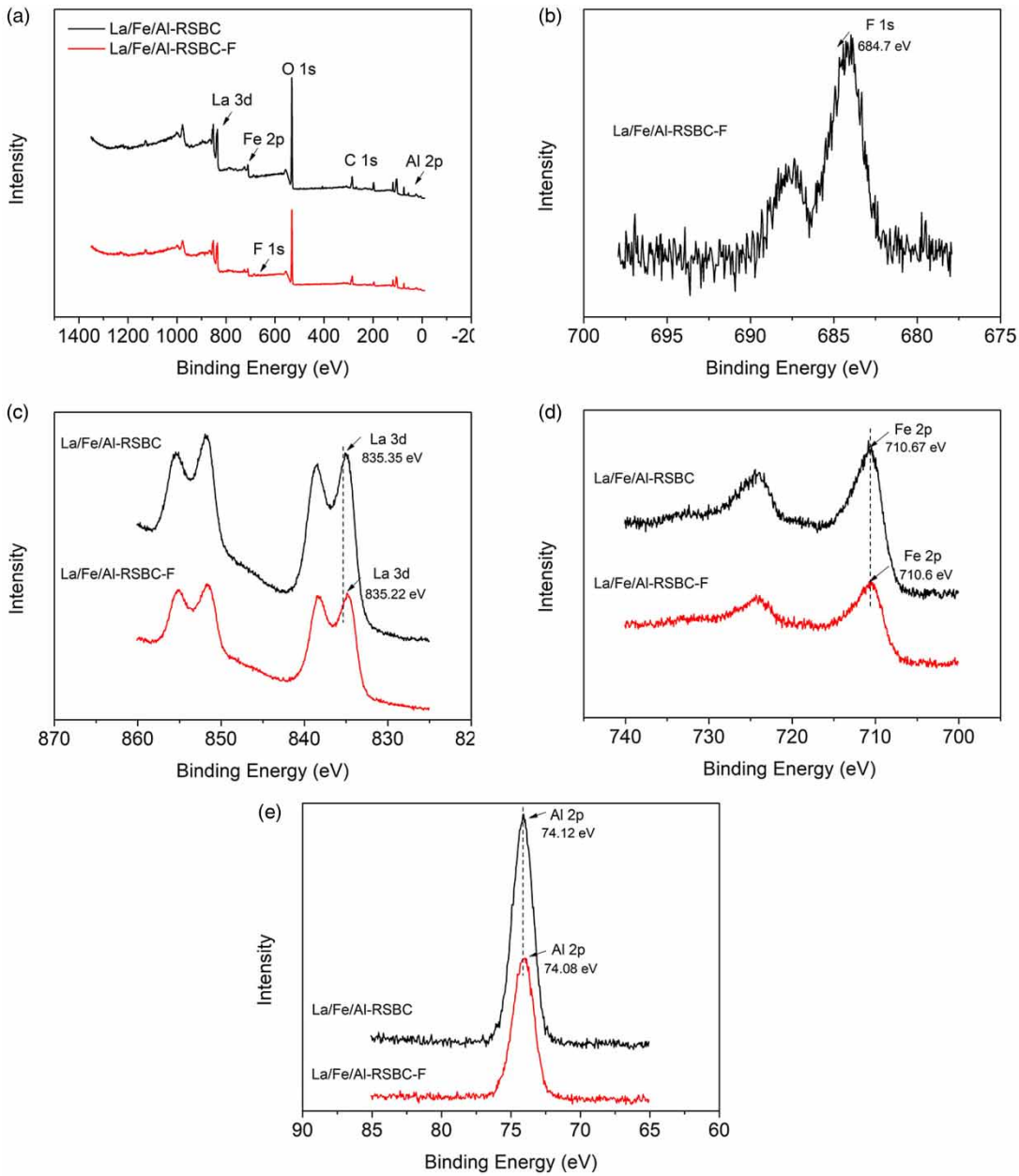

Figure 9 | (a) Wide scan spectra of the La/Fe/Al-RSBC adsorbent and F-loaded adsorbent; high resolution XPS spectra of (b) F 1 s, (c) La 3d before and after adsorption, (d) Fe 2p before and after adsorption, (e) Al 2p before and after adsorption.

Table 5 | Atomic ratios of La/Fe/Al-RSBC before and after fluoride adsorption obtained from XPS analysis

	Atomic ratio %						
Adsorbent	**C**	**O**	**La**	**Fe**	**Al**	**F**	**Total**
La/Fe/Al-RSBC	21.25	57.24	4.57	4.55	12.39	0	100
La/Fe/Al-RSBC-F	24.20	54.84	4.03	3.76	11.34	1.82	100

and Al oxide, and that a synergistic interaction between Fe and Al oxide, Fe and La oxide occurred during the defluorination process, which led to higher adsorption performance and broader pH application range of La/Fe/Al-RSBC. Thus, a mechanism for the La/Fe/Al-RSBC adsorption was proposed as illustrated in Figure 10.

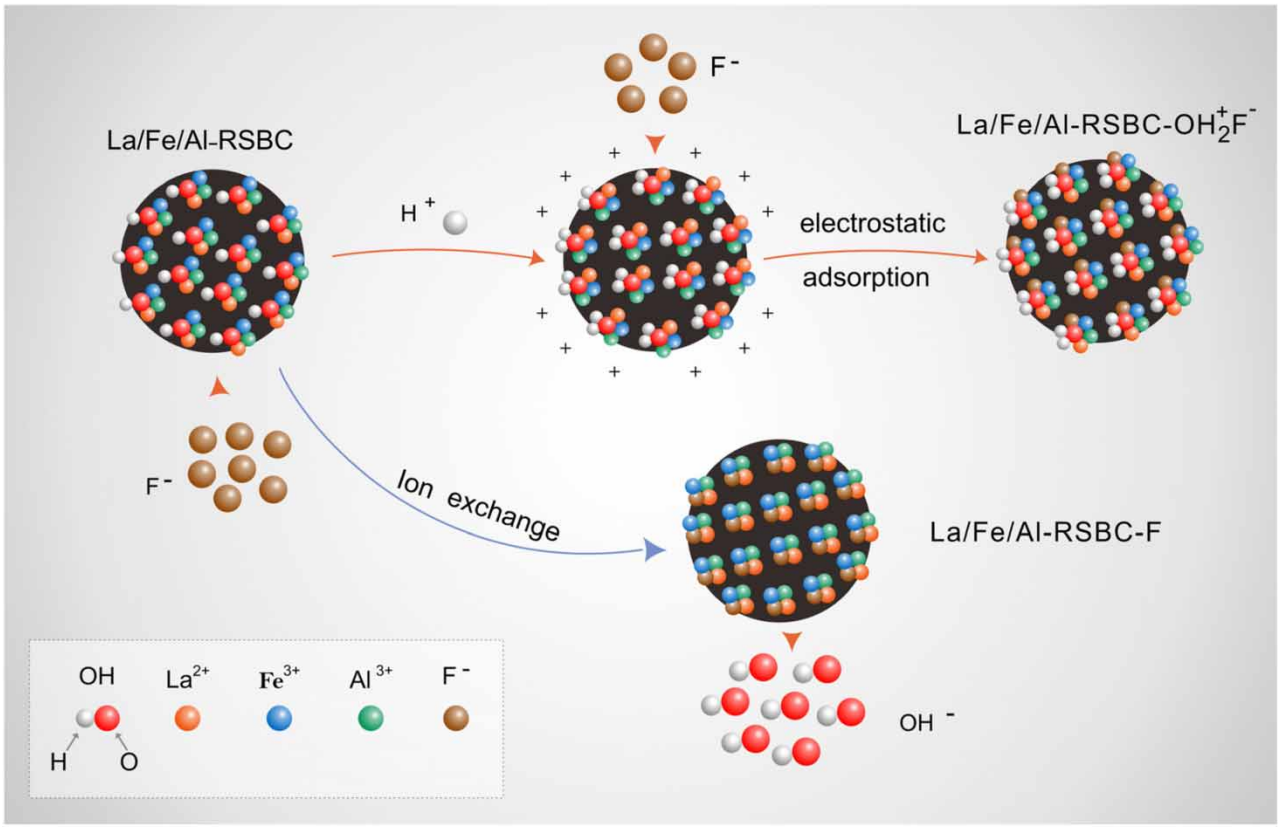

Figure 10 | Possible fluoride adsorption mechanism of La/Fe/Al-RSBC.

The mechanism of fluoride adsorption by La/Fe/Al-RSBC could follow a two-step reaction (Figure 10) similar to that already reported (Cai *et al.* 2015). In the acidic pH range, the hydroxyl groups produced by amorphous lanthanum hydroxide and aluminum hydroxide including high poly-aluminum on the surface of the adsorbent could be protonated to be positive, and metallic cations at the surface of La/Fe/Al-RSBC could also contribute to the positive surface charge. The positively charged surface sites on the surface of La/Fe/Al-RSBC attracted the negatively charged fluoride ions by electrostatic interaction and formed a strong covalent chemical bond (Figure 10) (Na & Park 2010). Due to the dispersion of biochar and the stability of poly-aluminum or other metallic cations, the adsorbent remained positively charged in the high pH range and hence the electrostatic adsorption could still be maintained. When pH >7.0, the adsorption of fluoride by La/Fe/Al-RSBC could occur by an ion exchange reaction between hydroxyl and fluoride ions (Figure 10) (Chen *et al.* 2017). It could be concluded from the calculated average free energy of adsorption (E) that the main mechanism was ligand exchange. It was evident that ternary metals played a synergistic role, and biochar acted as a carrier and dispersion. Lanthanum oxide and aluminum oxide were responsible for adsorption of fluoride, while iron oxide and biochar were responsible for broadening the pH range by bimetallic Fe-O-Al and Fe-O-La bonds formation in metals loading on RSBC progress (Cai *et al.* 2015). Thus, fluoride would likely be located fully on the surface, indicating that the La/Fe/Al-RSBC adsorbent had the particular advantages of both great fluoride adsorption capacity and wide applicable pH range.

The reaction that occurs during the adsorption process could be described as:

$$\equiv \mathrm{MOH} + \mathrm{H}^{+} \rightarrow \mathrm{MOH}_2^{+}$$

$$\equiv \mathrm{MOH}_2^{+} + \mathrm{F}^{-} \rightarrow \mathrm{MOH}_2^{+}\mathrm{F}^{-}$$

$$\equiv \mathrm{MOH}^{n+} + \mathrm{xF}^{-} \rightarrow \mathrm{MOHF}^{(n-x)^{+}}$$

$$\equiv \mathrm{MOH} + \mathrm{F}^{-} \rightarrow \mathrm{MF} + \mathrm{OH}^{-}$$

where ≡M represented the metal on the surface of La/Fe/Al-RSBC absorbent.

CONCLUSION

A low-cost and high-efficiency novel cost-effective adsorbent was developed by loading La/Fe/Al oxides onto RSBC through a co-precipitation method to remove fluoride from drinking water. La/Fe/Al-RSBC exhibited superior fluoride removal performance over other biochar adsorbents with a maximum adsorption capacity of 111.11 mg/g. The fluoride adsorption on the La/Fe/Al-RSBC adsorbent followed the Langmuir isotherm model and pseudo-second-order kinetic model, whereas fluoride adsorption on the raw RSBC followed the Freundlich isotherm model. Electrostatic adsorption and ion exchange were the dominant mechanisms for the defluoridation by La/Fe/Al-RSBC. The presence of coexisting anions Cl^-, SO_4^{2-}, NO_3^-, and HCO_3^- had little effect on the removal of fluoride. The fluoride removal rate could be maintained after three regeneration cycles. Furthermore, solution pH could little affect the fluoride removal by La/Fe/Al-RSBC, with an optimum pH range from 3.0 to 11.0. In short, La/Fe/Al-RSBC had great potential in practical application due to its efficient, wide pH range and reusable advantages.

ACKNOWLEDGEMENTS

This work was financially supported by the National Natural Science Foundation of China (No.51078348), the National College Students Innovation, Entrepreneurship Training Program (No. 201910304035Z, No. 2020132) and Nantong Science and technology project (MS12020076).

DATA AVAILABILITY STATEMENT

All relevant data are included in the paper or its Supplementary Information.

REFERENCES

Abri, A., Tajbakhsh, M. & Sadeghi, A. 2019 Adsorption of fluoride on a chitosan-based magnetic nanocomposite: equilibrium and kinetics studies. *Water Science & Technology* **19** (1–2), 40–51.

Ajisha, M. A. T. & Rajagopal, K. 2014 Characterization and adsorption study using *cocus nucifera* midribs for fluoride removal. *Journal of the Institution of Engineers* **94** (4), 209–217.

Ahmed, M. B., Zhou, J. L., Ngo, H. H., Guo, W. & Chen, M. 2016 Progress in the preparation and application of modified biochar for improved contaminant removal from water and wastewater. *Bioresource Technology* **214**, 836–851.

Awual, M. R., Yaita, T., Shiwaku, H. & Suzuki, S. 2015 A sensitive ligand embedded nano-conjugate adsorbent for effective cobalt(II) ions capturing from contaminated water. *Chemical Engineering Journal* **276**, 1–10.

Bakhtiari, N. & Azizian, S. 2015 Adsorption of copper ion from aqueous solution by nanoporous MOF-5: a kinetic and equilibrium study. *Journal of Molecular Liquids* **206**, 114–118.

Bansiwal, A., Thakre, D., Labhshetwar, N., Meshram, S. & Rayalu, S. 2009 Fluoride removal using lanthanum incorporated chitosan beads. *Colloids & Surfaces B Biointerfaces* **74** (1), 216–224.

Bhatnagar, A., Kumar, E. & Sillanp, M. 2011 Fluoride removal from water by adsorption – A review. *Chemical Engineering Journal* **171** (3), 811–840.

Cai, H.-m., Chen, G.-j., Peng, C.-y., Zhang, Z.-z., Dong, Y.-y., Shang, G.-z., Zhu, X.-h., Gao, H.-j. & Wan, X.-c. 2015 Removal of fluoride from drinking water using tea waste loaded with Al/Fe oxides: a novel, safe and efficient biosorbent. *Applied Surface Science* **328**, 34–44. doi:10.1016/j.apsusc.2014.11.164.

Chai, L., Wang, Y., Zhao, N., Yang, W. & You, X. 2013 Sulfate-doped Fe_3O_4/Al_2O_3 nanoparticles as a novel adsorbent for fluoride removal from drinking water. *Water Research* **47** (12), 4040–4049.

Chen, G. J., Peng, C. Y., Fang, J. Y., Dong, Y. Y., Zhu, X. H. & Cai, H. M. 2016 Biosorption of fluoride from drinking water using spent mushroom compost biochar coated with aluminum hydroxide. *Desalination Water Treatment* **57** (26), 12385–12395.

Chen, P., Wang, T., Xiao, Y., Tian, E., Wang, W., Zhao, Y., Tian, L., Jiang, H. & Luo, X. 2017 Efficient fluoride removal from aqueous solution by synthetic Fe-Mg-La tri-metal nanocomposite and the analysis of its adsorption mechanism. *Journal of Alloys & Compounds* **738**, 118–129.

Cui, H., Li, Q., Qian, Y., Tang, R., An, H. & Zhai, J. 2011 Defluoridation of water via electrically controlled anion exchange by polyaniline modified electrode reactor. *Water Research* **45** (17), 5736–5744.

Delgadillo-Velasco, L., Hernández-Montoya, V., Cervantes, F. J., Montes-Morán, M. A. & Lira-Berlanga, D. 2017 Bone char with antibacterial properties for fluoride removal: preparation, characterization and water treatment. *Journal of Environmental Management* **201**, 277–285.

Dong, S. & Wang, Y. 2016 Characterization and adsorption properties of a lanthanum-loaded magnetic cationic hydrogel composite for fluoride removal. *Water Research* **88**, 852–860.

Farrah, H., Slavek, J. & Pickering, W. F. 1987 Fluoride interactions with hydrous aluminum oxides and alumina. *Australian Journal of Soil Research* **25** (1), 55–69.

Fu, Y., Shen, Y., Zhang, Z., Ge, X. & Chen, M. 2018 Activated bio-chars derived from rice husk via one- and two-step KOH-catalyzed pyrolysis for phenol adsorption. *Science of the Total Environment* **646**, 1567–1577.

Ganvir, V. & Das, K. J. J. o. H. M. 2011 Removal of fluoride from drinking water using aluminum hydroxide coated rice husk ash. *Journal of Hazardous Materials* **185** (2–3), 1287–1294.

Habibi, N., Rouhi, P. & Ramavandi, B. 2018 Modification of *tamarix hispida* biochar by lanthanum chloride for enhanced fluoride adsorption from synthetic and real wastewater. *Environmental Progress and Sustainable Energy* **38** (s1), 298–305.

Ho, Y.-S. 2006 Review of second-order models for adsorption systems. *Journal of Hazardous Materials* **136**, 681–689.

Ho, Y. S. & Mckay, G. 1998 A comparison of chemisorption kinetic models applied to pollutant removal on various sorbents. *Process Safety & Environmental Protection* **76** (4), 332–340.

Ho, Y. S. & Mckay, G. 2000 The kinetics of sorption of divalent metal ions onto sphagnum moss peat. *Water Research* **34** (3), 735–742.

Jain, S. & Jayaram, R. V. 2009 Removal of fluoride from contaminated drinking water using unmodified and aluminium hydroxide impregnated blue lime stone waste. *Separation Science & Technology* **44** (6), 1436–1451.

Jian, Z., Zhu, W., Jie, Y., Zhang, H., Zhang, Y., Lin, X. & Luo, X. 2018 Highly selective and efficient removal of fluoride from ground water by layered Al-Zr-La Tri-metal hydroxide. *Applied Surface Science* **435**, 920–927.

Jiang, H., Li, X., Tian, L., Wang, T., Wang, Q., Niu, P., Chen, P. & Luo, X. 2019 Defluoridation investigation of Yttrium by laminated Y-Zr-Al tri-metal nanocomposite and analysis of the fluoride sorption mechanism. *Science of the Total Environment* **648** (PT.839–1672), 1342–1353.

Lahnid, S., Tahaikt, M., Elaroui, K., Idrissi, I., Hafsi, M., Laaziz, I., Amor, Z., Tiyal, F. & Elmidaoui, A. 2008 Economic evaluation of fluoride removal by electrodialysis. *Desalination* **230** (1–3), 213–219.

Lawrinenko, M., Laird, D., Banik, A. & Laird, D. A. 2017 *Aluminum and Iron Biomass Pretreatment Impacts on Biochar Anion Exchange Capacity*.

Ling, Z., Qi, Z., Liu, J., Ning, C., Wan, L. & Chen, J. 2012 Phosphate adsorption on lanthanum hydroxide-doped activated carbon fiber. *Chemical Engineering Journal* **185–186**, 160–167.

Liu, R., Scott, N. & Chen, T. 2016 Characterization of energy carriers obtained from the pyrolysis of white ash, switchgrass and corn stover – Biochar, syngas and bio-oil. *Fuel Processing Technology* **142**, 124–134.

Loganathana, P., Vigneswarana, S., Kandasamya, J. & Naidub, R. 2013 Defluoridation of drinking water using adsorption processes. *Journal of Hazardous Materials* **248–249**, 1–19.

Mahramanlioglu, M., Kizilcikli, I. & Bier, I. 2002 Adsorption of fluoride from aqueous solution by acid treated spent bleaching earth. *Journal of Fluorine Chemistry* **115** (1), 41–47.

Maliyekkal, S. M., Shukla, S., Philip, L. & Nambi, I. M. 2008 Enhanced fluoride removal from drinking water by magnesia-amended activated alumina granules. *Chemical Engineering Journal* **140** (1–3), 183–192.

Medellin-Castillo, N. A., Leyva-Ramos, R., Padilla-Ortega, E., Perez, R. O., Flores-Cano, J. V. & Berber-Mendoza, M. S. 2014 Adsorption capacity of bone char for removing fluoride from water solution. Role of hydroxyapatite content, adsorption mechanism and competing anions. *Journal of Industrial & Engineering Chemistry* **20** (6), 4014–4021.

Meenakshi & Maheshwari, R. C. 2006 Fluoride in drinking water and its removal. *Journal of Hazardous Materials* **137** (1), 456–463.

Mei, L., Qiao, H., Ke, F., Peng, C., Hou, R., Wan, X. & Cai, H. 2020 One-step synthesis of zirconium dioxide-biochar derived from *camellia oleifera* seed shell with enhanced removal capacity for fluoride from water. *Applied Surface Science* **509**, 144685.

Mian, M. M. & Liu, G. 2018 Recent progress in biochar-supported photocatalysts: synthesis, role of biochar, and applications. *Rsc Advances* **8** (26), 14237–14248.

Na, C. K. & Park, H. J. 2010 Defluoridation from aqueous solution by lanthanum hydroxide. *Journal of Hazardous Materials* **183** (1–3), 512–520.

Pant, K. K. 2004 Investigations on the column performance of fluoride adsorption by activated alumina in a fixed-bed. *Chemical Engineering Journal* **98** (1–2), 165–173.

Peng, F., Deng, S., Luo, T. & Yang, X. 2017 A new adsorbent of a Ce ion-implanted metal-organic framework (MIL-96) with high-efficiency Ce utilization for removing fluoride from water. *Dalton Transactions* **46** (6), 1996–2006.

Pietrelli, L. 2005 Fluoride wastewater treatment by adsorption onto metallurgical grade alumina. *Annali Di Chimica* **95** (5), 303–312.

Piyush, K., Pandey, M. & Sharma, R. 2012 Defluoridation of water by a biomass: *tinospora cordifolia*. *Journal of Environmental Protection* **3** (7), 610–616.

Rajkumar, S., Murugesh, S., Sivasankar, V., Darchen, A., Msagati, T. A. M. & Chaabane, T. 2015 Low-cost fluoride adsorbents prepared from a renewable biowaste: syntheses, characterization and modeling studies. *Arabian Journal of Chemistry* **12** (8), 3004–3017.

Ruan, Z., Tian, Y., Ruan, J., Gui, G., Iqbal, K., Iqbal, A. & Yan, S. 2017 Synthesis of hydroxyapatite/multi-walled carbon nanotubes for the removal of fluoride ions from solution. *Applied Surface Science* **412**, 578–590.

Tangsir, S., Hafshejani, L. D., Lhde, A., Maljanen, M. & Bhatnagar, A. 2016 Water defluoridation using Al_2O_3 nanoparticles synthesized by flame spray pyrolysis (FSP) method. *Chemical Engineering Journal* **288**, 198–206.

Wang, Y. & Reardon, E. J. 2001 Activation and regeneration of a soil sorbent for defluoridation of drinking water. *Applied Geochemistry* **16** (5), 531–539.

Wang, J., Kang, D., Yu, X., Ge, M. & Chen, Y. 2015 Synthesis and characterization of Mg–Fe–La trimetal composite as an adsorbent for fluoride removal – ScienceDirect. *Chemical Engineering Journal* **264**, 506–513.

Wang, J., Wang, X., Tian, L., Chen, Y., Hayat, T., Hu, J., Alsaedi, B., Guo, W. & Wang, X. 2016 Performances and mechanisms of Mg/Al and Ca/Al layered. double hydroxides for graphene oxide removal from aqueous solution. *Chemical Engineering Journal* **297**, 106–115.

Wang, A., Zhou, K., Liu, X., Liu, F., Zhang, C. & Chen, Q. 2017a Granular tri-metal oxide adsorbent for fluoride uptake: adsorption kinetic and equilibrium studies. *Journal of Colloid & Interface Science* **505**, 947–955.

Wang, J., Chen, N., Li, M. & Feng, C. 2017b Efficient removal of fluoride using polypyrrole-modified biochar derived from slow pyrolysis of pomelo peel: sorption capacity and mechanism. *Journal of Polymers & the Environment* **26** (4), 1559–1572.

Wang, J., Wu, L., Li, J., Tang, D. & Zhang, G. 2018a Simultaneous and efficient removal of fluoride and phosphate by Fe-La composite: adsorption kinetics and mechanism. *Journal of Alloys and Compounds* **753**, 422–432.

Wang, J., Chen, N., Feng, C. & Li, M. 2018b Performance and mechanism of fluoride adsorption from groundwater by lanthanum-modified pomelo peel biochar. *Environmental Science & Pollution Research* **25** (16), 1–10.

Wen, D., Zhang, F., Zhang, E., Wang, C., Han, S. & Zheng, Y. 2013 Arsenic, fluoride and iodine in groundwater of China. *Journal of Geochemical Exploration* **135**, 1–21.

Yadav, A. K., Abbassi, R., Gupta, A. & Dadashzadeh, M. 2013a Removal of fluoride from aqueous solution and groundwater by wheat straw, Sawdust and activated bagasse carbon of sugarcane. *Ecological Engineering* **62**, 211–218.

Yadav, A. K., Abbassi, R., Gupta, A. & Dadashzadeh, M. J. E. E. 2013b Removal of fluoride from aqueous solution and groundwater by wheat straw, sawdust and activated bagasse carbon of sugarcane *Ecological Engineering* **52**, 211–218.

Yan, L., Gu, W., Zhou, N., Ye, C. & Yang, Y. 2021 Preparation and characterization of wheat straw biochar loaded with aluminum/ lanthanum hydroxides: a novel adsorbent for removing fluoride from drinking water. *Environmental Technology* **1903563**, 1–29.

Zhang, Y. & Huang, K. 2019 Grape pomace as a biosorbent for fluoride removal from groundwater. *RSC Advances* **9** (14), 7767–7776.

Zhang, T., Li, Q., Xiao, H., Lu, H. & Zhou, Y. 2012 Synthesis of Li–Al layered double hydroxides (LDHs) for efficient fluoride removal. *Industrial Engineering Chemistry Research* **51** (35), 11490–11498.

Zhang, S., Lu, Y., Lin, X., Su, X. & Zhang, Y. 2014 Removal of fluoride from groundwater by adsorption onto La(III)- Al(III) loaded scoria adsorbent. *Applied Surface Science* **303**, 1–5.

Zhang, Z., Yan, L., Yu, H., Yan, T. & Li, X. 2019 Adsorption of phosphate from aqueous solution by vegetable biochar/layered double oxides: fast removal and mechanistic studies. *Bioresource Technology* **284**, 65–71.

Zhou, J., Liu, Y., Han, Y., Jing, F. & Chen, J. 2019 Bone-derived biochar and magnetic biochar for effective removal of fluoride in groundwater: effects of synthesis method and coexisting chromium. *Water Environment Research* **91**, 588–597.

First received 3 December 2020; accepted in revised form 11 July 2021. Available online 23 July 2021